MODEL STUDY OF WAVE PROPAGATION IN A CONTINUOUS ICE SHEET

OTTAR HELGE GRANDE

CANADIAN THESES ON MICROFICHE

I.S.B.N.

THESES CANADIENNES SUR MICROFICHE

National Library of Canada
Collections Development Branch

Canadian Theses on
Microfiche Service

Ottawa, Canada
K1A 0N4

Bibliothèque nationale du Canada
Direction du développement des collections

Service des thèses canadiennes
sur microfiche

NOTICE

The quality of this microfiche is heavily dependent upon the quality of the original thesis submitted for microfilming. Every effort has been made to ensure the highest quality of reproduction possible.

If pages are missing, contact the university which granted the degree.

Some pages may have indistinct print especially if the original pages were typed with a poor typewriter ribbon or if the university sent us a poor photocopy.

Previously copyrighted materials (journal articles, published tests, etc.) are not filmed.

Reproduction in full or in part of this film is governed by the Canadian Copyright Act, R.S.C. 1970, c. C-30. Please read the authorization forms which accompany this thesis.

THIS DISSERTATION
HAS BEEN MICROFILMED
EXACTLY AS RECEIVED

AVIS

La qualité de cette microfiche dépend grandement de la qualité de la thèse soumise au microfilmage. Nous avons tout fait pour assurer une qualité supérieure de reproduction.

S'il manque des pages, veuillez communiquer avec l'université qui a conféré le grade.

La qualité d'impression de certaines pages peut laisser à désirer, surtout si les pages originales ont été dactylographiées à l'aide d'un ruban usé ou si l'université nous a fait parvenir une photocopie de mauvaise qualité.

Les documents qui font déjà l'objet d'un droit d'auteur (articles de revue, examens publiés, etc.) ne sont pas microfilmés.

La reproduction, même partielle, de ce microfilm est soumise à la Loi canadienne sur le droit d'auteur, SRC 1970, c. C-30. Veuillez prendre connaissance des formules d'autorisation qui accompagnent cette thèse.

LA THÈSE A ÉTÉ
MICROFILMÉE TELLE QUE
NOUS L'AVONS REÇUE

NL-339 (r. 82/08)

Canada

MODEL STUDY OF WAVE PROPAGATION IN A CONTINUOUS ICE SHEET

by

© Ottar Helge Grande, Siv.ing, MNIF

A thesis submitted in partial fulfillment of
the requirements for the degree of

Master of Engineering

Faculty of Engineering and Applied Science
Memorial University of Newfoundland

July 1983

St. John's Newfoundland, Canada

ABSTRACT

The propagating and amplitude attentuating features of gravity waves in ice covered water has, during the last decase, been given a fairly extensive theoretical treatment. Usually the wave characteristics have been estimated by modelling the ice cover as a continuous linear elastic or linear visco elastic plate of uniform thickness on an elastic foundation.

In order to determine the validity of the theoretically derived dispersion relationships for the propagation and attenuation of gravity waves entering an ice field a laboratory study was conducted. Continuous semi-infinite artificial ice sheets based on polypropylene pellet and wax combinations were used and the wavelengths and wave amplitudes were measured. Theoretical values for the wavelengths were obtained by solving the wave dispersion equation using Padé coefficients and compared with the experimentally obtained values. The wave amplitudes in the ice covered region were calculated from the wave energy.

ACKNOWLEDGMENT

The author wishes to thank his supervisor, Dr. D.B. Muggeridge, for his guidance during the work finalized in this thesis and Dr. V.M. Arunachalam for many fruitful discussions regarding the theoretical part of this thesis. Excellent help was provided by Mr. Gerald Guy in conducting the experiments. Furthermore, I would like to thank Acres Consulting Services Limited for their permission to use their model ice. The financial support provided by the School of Graduate Studies of Memorial University of Newfoundland is also gratefully acknowledged. Financial support to carry out the experiments was provided by the Natural Sciences and Engineering Research Council of Canada through Grant G0561 to Memorial University of Newfoundland.

TABLE OF CONTENTS

LIST OF FIGURES

NOMENCLATURE

A	-	Wave amplitude
A_w	-	Wave amplitude in open water
A_i	-	Wave amplitude in ice covered water
$_oA_i$	-	Wave amplitude at the ice edge
$A_i(x)$	-	Wave amplitude at a distance x into the ice cover
$\|A_j\|$, $\|B_j\|$		Potential amplitudes inside the ice cover
B	-	Flow law parameter
D	-	Plate rigidity
E	-	Modulus of elasticity for ice
I_n	-	Function defined as: $\frac{1}{\pi}\int_0^{\pi} \sin^{q+1}\beta d\beta$
K	-	Function defined as: $2\left(\frac{4\pi^2 E}{(1-\nu^2)}\right)^{q+1} \frac{1}{(2<B>)^q (q+2)}$
$\|P\|$	-	Potential amplitude of incident wave
Q	-	Function defined as: $1+\frac{32Eh^3\pi^4}{3\rho_w g\lambda_i^4(1-\nu^2)}$
$\|R\|$	-	Potential amplitude of reflected wave
S	-	Function defined as: $\frac{Kh^{q+2}I_n}{\lambda_i^{2q+2}\rho_w gUQ}$
T	-	Wave period
U	-	Group velocity of wave in ice covered water
U_w	-	Group velocity of wave in open water
b	-	Width of beam
d	-	Water depth
g	-	Gravitational acceleration
$<B>$	-	Average value of B

h	-	Half the ice thickness
k, k_o, k_1, k_2		Wave number, $2\pi/\lambda$
kei	-	Kelvin function
l_b	-	Breaking length
ℓ_{c1}	-	Characteristic length for beam
ℓ_{c2}	-	Characteristic length for plate
n	-	Geometric scaling factor
q	-	Flow law exponent
r	-	Distance from point of loading to point of measured deflection
t	-	Time
W_2	-	Vertical ice cover displacement
x, y, z	-	Cartesian coordinates
¶	-	Function defined as: $\frac{\cosh(az+ad+i(bz+bd))}{\cosh(ad+ibd)}$
Φ	-	Velocity potential
Ω	-	Function defined as: $\frac{\cosh(az+ad-i(bz+bd))}{\cosh(ad-ibd)}$
δ	-	Deflection
δp	-	Excess of pressure just beneath the ice-water interface over the atmospheric pressure
λ_i	-	Wavelength inside the ice cover
λ_o	-	Open water wave length
ν	-	Poisson's ratio
ρ_i	-	Density of ice

ρ_w - Density of water

σ_f - Flexural strength of ice

ω - Circular wave frequency, $2\pi/T$

1. INTRODUCTION

The increase in offshore activities in ice infested waters during the last decades has resulted in a demand for better understanding of the properties of water waves in ice covered seas.

From an engineering viewpoint it is of importance to be able to predict the wave motion at any location and at any time inside an ice cover, both to evaluate structures located in the ice field and to estimate the possibilities for ice break up due to wave motion. Also if any kind of refraction analysis is to be carried out the dispersion equation for waves within the ice cover has to be known.

Published literature on the mathematical modelling of the interaction of gravity waves with floating sheets of ice include such work as Wadhams' (1973) where the ice sheet is treated as an elastic plate floating with zero submergence on an incompressible fluid of infinite depth. This work was extended by Carter (1978) to include the finite water depth case. Bates and Shapiro (1980a, 1980b), however, analyzed the problem by treating the fluid to be compressible and the ice sheet to be an elastic laterally compressed plate floating with zero submergence on a fluid of finite depth. Squire and Allan (1980) and Bates and Shapiro (1981) treated the ice as a visco elastic plate floating on a perfect fluid. These studies involve the solution of a wave dispersion equation to obtain the wave characteristics of the flexural gravity waves.

Field data as well as laboratory data to verify the wave characteristics inside an ice sheet predicted from the various theories are very limited. As far as the author knows the only existing field data on the wave characteristics in a continuous ice cover is due to the field work done by Squire and Allan, (1980), near Twillingate off the northern coast of Newfoundland.

The only laboratory data on this problem are from the work done by Ofuya and Reynolds in 1967. As a modelling material they used thin polyethylene sheets to simulate an unbroken ice cover. Unfortunately the elastic modulus for this material is close to 1.1 GPa which corresponds to the range of values of elastic modulus, E, reported for sea ice, while the sheet thicknesses and input wave characteristics correspond more to a scale in the range of 1:100. No laboratory work has up to now been reported on this problem using model material for ice that obeys the scaling laws as summarized by Michel, (1978).

The amplitude attenuation inside a continuous ice cover has been given a fairly extensive theoretical treatment by Wadhams, (1973, 1983) for the deep water region while Carter, (1978), has extended this work to include the finite water depth region. Unfortunately no field data on the wave amplitude attenuating effect of a continuous ice cover exist to verify the proposed theory.

2. THEORETICAL CONSIDERATIONS

Consider an ice cover idealized as shown on Fig. 1. This semi-infinite plate of uniform thickness 2h, behaves elastically and has a modulus of elasticity E, Poisson's ratio ν and is floating with zero submergence in water of constant depth d. Furthermore it is assumed that small amplitude wave theory for monochromatic waves can be used, that the waves are incident normally on the straight leading edge of the ice cover, that the excess hydrodynamic pressure δp beneath the ice cover can be determined using the linearized form of Bernoulli's equation and that the equation of motion of the ice sheet can be expressed using small deformation plate theory. In addition the water is assumed to be inviscid and incompressible while the flow is assumed to be irrotational. A velocity potential Φ_n, satisfying Laplace's equation, will then exist in each of the regions shown on Fig. 1.

$$\nabla^2 \Phi_n = 0 \qquad n = 1,2 \qquad (2.1)$$

Eq. 2.1 is subjected to the boundary conditions:

$$\frac{\partial \Phi_n}{\partial z} = 0 \qquad \text{at } z = -d \qquad (2.2)$$

$$\frac{\partial W_n}{\partial t} - \frac{\partial \Phi_n}{\partial z} = 0 \qquad \text{at } z = 0 \qquad (2.3)$$

where x and z are horizontal and vertical coordinates, t is time, W_n is the free surface elevation above still water level in regions 1 and 2 and d is the still water depth.

In region 1 the linearized Bernoulli's equation at the free surface is given as:

$$\frac{1}{g}\frac{\partial \Phi_1}{\partial t} + W_1 = 0 \qquad \text{at } z = 0 \qquad (2.4)$$

A solution satisfying equations 2.1 to 2.4 is:

$$\Phi_1 = [P\, e^{ikx} + R\, e^{-ikx}]\, \frac{\cosh k(z+d)}{\cosh kd}\, e^{-i\omega t} \qquad (2.5)$$

where k is the wave number, ω is the circular wave frequency $|P|$ is the potential amplitude of the incident wave and $|R|$ is the potential amplitude of the wave reflected normally from the ice edge.

In region 2 the equation of motion of the plate is given as:

$$2h\, \rho_i \frac{\partial^2 W_2}{\partial t^2} = -D \frac{\partial^4 W_2}{\partial x^4} + \delta p \qquad (2.6)$$

where ρ_i is the ice density and D is the plate rigidity, defined as:

$$D = \frac{2h^3 E}{3(1-\nu^2)} \qquad (2.7)$$

The excess hydrodynamic pressure beneath the ice plate is obtained from the linearized Bernoulli's equation as:

$$\delta p = -\rho_w g W_2 - \rho_w \frac{\partial \Phi_2}{\partial t} \qquad \text{at } z = 0 \qquad (2.8)$$

A solution for Φ_2 can be chosen as a sum of potentials as given in eq. 2.9:

$$\Phi_2 = \sum_j [A_j e^{ik_j x} + B_j e^{-ik_j x}] \frac{\cosh k_j(z+d)}{\cosh k_j d} e^{-i\omega t} \qquad (2.9)$$

Combination of equations 2.1 to 2.3 and 2.6, 2.8 and 2.9 yields the dispersion equation in the ice covered region as:

$$D \tanh(k_j d) k_j^5 + \tanh(k_j d)(\rho_w g - 2h\rho_i \omega^2) k_j - \rho_w \omega^2 = 0 \qquad (2.10)$$

where j takes values from 1 to 5.

As a quintic polynomial equation with real coefficients, it will have one real and four complex roots, where two complex roots are the complex conjugate of the two others. Furthermore two of the complex roots are unrealistic since they lead to potentials that increase indefinitely with depth. The three feasible roots are:

$$\begin{aligned} k_o &= k_o \\ k_1 &= -a+ib \\ k_2 &= -a-ib \end{aligned} \qquad (2.11)$$

The real wave number, k_o, represents the flexural-gravity wave, and its characteristics were obtained by solving the dispersion equation 2.10 by use of a simple iteration loop and by a numerical procedure using Padé coefficients as described by Arunachalam et al (1983).

The velocity potential, Φ_2^1, represented by the complex wave numbers, k_1 and k_2, can, as shown in Appendix 1, be expanded and written as:

$$\Phi_2^1 = [2B_2(\P\Omega)^{\frac{1}{2}}\cos(ax-\theta)e^{-bx}+(A_1-B_2)\Omega e^{-(bx+iax)}]e^{-i\omega t} \quad (2.12)$$

where $\P$ and Ω is given as

$$\P = \frac{\cosh(az+ad+i(bz+bd))}{\cosh(ad+ibd)} \quad (2.13a)$$

$$\Omega = \frac{\cosh(az+ad-i(bz+bd))}{\cosh(ad-ibd)} \quad (2.13b)$$

$$\theta = \arctan\frac{i(\P-\Omega)}{\P+\Omega} \quad (2.13c)$$

The first term in eq. 2.12 is a standing wave with exponential decay with respect to the x-coordinate, and the nodes are defined by:

$$ax-\arctan\frac{i(\P-\Omega)}{\P+\Omega} = (2m-1)\frac{\pi}{2} \quad m=0,1,2... \quad (2.14)$$

The second term in eq. 2.12 represents an exponentially decaying progressive wave.

For the special case, $d\to\infty$, eq. 2.12 reduces to the velocity potential for infinite water depth as given by Wadhams (1983):

$$\Phi_2^1 = [2B_2\cos(ax+bz)+(A_1-B_2)e^{-i(ax+bz)}]e^{-(bx-az)}e^{-i\omega t} \quad (2.15)$$

From eq. 2.15 it is seen that the decaying progressive wave represents wave energy that propagates diagonally upwards from the boundary plane between region 1 and region 2, and given to the ice cover as increased kinetic energy near the ice edge.

2.1 Damping of Waves at the Ice Edge

In open water the wave energy is transported in the water column while in ice covered water the wave energy transport is shared between the ice and the water. This difference in energy transport results in an instantaneous reduction of the open water wave amplitude, A_w, to wave amplitude $_oA_i$ at the ice edge. The wave amplitude, $_oA_i$, can be found in terms of A_w by requiring that the average rate of energy transmission, in the propagation direction of the wave, per unit width across the wavefront is the same in the open water region as in the ice covered region. By applying this approach $_oA_i$ will, according to Carter (1978), be given as shown in Eq. 2.16.

$$\left(\frac{A_w}{{}_oA_i}\right)^2 = \frac{U}{U_w}\left(1+\frac{Dk_o^4}{\rho_w g}\right) \tag{2.16}$$

where U is the group velocity of the flexural gravity wave, U_w is the group velocity in open water and g is the acceleration due to gravity.

2.2 Wave Attenuation within an Ice Cover

Due to the cyclic stresses induced in an ice cover by propagating flexural gravity waves the visco-elastic nature of the material ice results in an energy loss due to creep. The amplitude decay as a function of penetrated distance, x, into the ice cover can then be estimated by assuming that the creep energy loss is the major energy loss and can be derived from Nye's flow law. Wadhams (1973) has shown that by applying

this theory the amplitude at any given distance into the ice cover can be calculated from eq. 2.17 or 2.18:

$$A_i(x) = \frac{1}{(q-1)\ S\ x + ({}_oA_i)^{-(q-1)}}^{-(q-1)} \qquad \text{for } q>1 \qquad (2.17)$$

or

$$A_i(x) = {}_oA_i\, e^{-Sx} \qquad \text{for } q=1 \qquad (2.18)$$

where ${}_oA_i$ is given by eq. 2.16, q is the flow law exponent and S is a rather complex function of ice cover thickness and the visco-elastic properties of ice and of the wave characteristics of the propagating waves. Details of this function can be found in Carter (1978) and Wadhams (1973, 1983) and in the nomenclature.

3. SCALING LAWS

In order to scale from model to prototype, the laws of dynamic, geometric and kinematic similitude must be satisfied. Complete similitude is always the goal in physical modelling, but in practice it is very seldom obtained. But by making sure that the effect of factors that are not properly scaled are of secondary importance in model as well as in prototype we can obtain a reasonably good model without having complete similitude.

In the present model the commonly used assumption that for free surface flow gravitational and inertia forces are of prime importance while viscous forces are of secondary importance is applied. Dynamic similitude is then obtained by holding the ratio of gravity forces to inertia forces constant. This results in what is known as Froude number scaling, defined as:

$$\left[\frac{V_m^2}{g_m . L_m}\right]^{\frac{1}{2}} = \left[\frac{V_p^2}{g_p . L_p}\right]^{\frac{1}{2}} \qquad (3.1)$$

where V and L are a characteristic velocity and length, g is acceleration due to gravity, and m and p denote model and prototype values respectively. Eq. 3.1 yields the following scaling factors between prototype and model values as long as the gravitational field is the same in model as in prototype.

Geometric similitude (Geometric scaling): $\frac{L_p}{L_m} = n$ (3.2a)

Kinematic similitude (Time scaling) : $\frac{V_p}{V_m} = n^{\frac{1}{2}}$ (3.2b)

Dynamic similitude (Force scaling) : $\frac{F_p}{F_m} = n^3$ (3.2c)

To model flexural forces properly as is required for this problem the Cauchy number has to be the same in model and in prototype. This yields:

$$\frac{V_m^2 \rho_m}{E_m} = \frac{V_p^2 \rho_p}{E_p} \tag{3.3}$$

Thus, for the same fluid this requires:

$$\frac{E_p}{E_m} = n \tag{3.4}$$

This implies that the rigidity, D, of the model ice cover is scaled according to the geometric scale. To study the breakup of a continuous sheet the flexural force F_b at fracture must be scaled. According to Michel (1978) this force can be expressed as:

$$F_b = \sigma_f h^2 C(\frac{a}{\ell}, \frac{b}{\ell}, \frac{c}{\ell}, \nu) \tag{3.5}$$

where a, b and c are representative lengths, ℓ is the characteristic length given by eq. 3.14, ν is Poisson's ratio, h is proportional to the sheet thickness, σ_f is the bending strength and C is a constant. By applying the scaling requirements derived in eq. 3.2a to c we obtain

$$\frac{\sigma_{fp}}{\sigma_{fm}} = n \qquad (3.6)$$

and

$$\frac{\ell_p}{\ell_m} = n \qquad (3.7)$$

The significance of a correctly scaled characteristic length is that all pieces broken by flexure in the model are scaled according to the geometric scaling factor.

3.1 Model Ice

Simulation of the ice cover in the present experimental program was accomplished using a polypropylene pellet, wax and oil mixture. This model ice, originally developed by ACRES Consulting Services Limited, has been found to reproduce some of the scaled mechanical properties of saline ice. The 3 mm diameter polypropylene pellets essentially control the thickness of the model ice, while the wax/oil mixture provides cohesion and strength to the material. Hence, by suitably adjusting the smount of pellets, wax and oil, an artificial ice sheet of the desired mechanical properties was obtained.

3.2 Ice growth

The ice cover was formed by applying a uniform layer of polypropylene pellets to the water surface. This layer was then sprayed with a warm liquid mixture of parowax and oil using a standard steel canister garden sprayer. This process

was repeated until the desired thickness was obtained. For example, to obtain an ice thickness of 11 and 18 mm, 3 and 6 layers of pellets were respectively used.

3.3 Characterization tests

A set of experiments to determine the modulus of elasticity, E, and the bending strength, σ_f, as a function of the amount of pellets, wax and oil used was done by producing several sheets of size 0.5 m x (1.2-1.6) m with different thicknesses. The sheets were cut into beams of approximately 0.1 m width and 1.2 - 1.6 m length. The beams were loaded to failure by applying a concentrated strip load at one of the ends. The thickness, 2h, and width, b, of the beams as well as the length, l_b, of the broken pieces and applied loads, P, were measured. By treating the beams as semi-infinite beams on elastic foundation, having uniform properties and behaving as a perfect elastic material the failure of the beams will be located at the point of maximum bending moment.

From the theoretical bending moment distribution as given by Hetényi (1946), the breaking length, l_b, can be related to the beam's characteristic lengths, ℓ_{cl}, as given in eq. 3.8.

$$l_b = \frac{\pi}{4} \ell_{cl} \tag{3.8}$$

where ℓ_{cl} is given as:

$$\ell_{cl} = \left(\frac{4EI}{\rho_w g}\right)^{\frac{1}{4}} \tag{3.9}$$

and I is the moment of inertia per unit width.

Eq. 3.8 and 3.9 in combination with the bending moment distribution yields expressions 3.10 and 3.11 that were used in calculating the modulus of elasticity, E, and the bending strength, σ_f.

$$E = (\frac{4}{\pi}l_b)^4 \frac{3\rho_w g(1-\nu^2)}{8h^3} \qquad (3.10)$$

$$\sigma_f = \frac{6Pl_b(1-\nu^2)}{\pi bh^2} \quad e^{-\frac{\pi}{4}} \sin\frac{\pi}{4} \qquad (3.11)$$

The experimental results are summarized in Figures 2 and 3.

During the main experiments the bending strength, σ_f, and modulus of elasticity, E, were determined using a different technique. The bending strength was determined by loading cantilever beams cut in the ice-sheet to failure, Fig. 4. By neglecting the buoyancy effect the bending strength was calculated using eq. 3.12 as recommended by Schwartz et al (1981).

$$\sigma_f = \frac{3Pl}{2bh^2} \qquad (3.12)$$

where P = applied load, l = length of the beam, b = beam width and h is half the beam thickness.

By monitoring the deflection, δ, of the ice sheet at a known distance, r, from the theoretical point of loading where the deadweights were applied, the modulus of elasticity was determined from eq. 3.13, after Timco 1981, using an iterative process.

$$\delta = \frac{\hat{P}}{2\pi\rho_w g \ell_{c_2}^2} \; \text{kei}\left(\frac{r}{\ell_{c_2}}\right) \qquad (3.13)$$

where kei is a Kelvin function and ℓ_{c_2} is the characteristic length for a plate given by eq. 3.14

$$\ell_{c_2} = \left[\frac{2Eh^3}{3\rho_w(1-\nu^2)g}\right]^{\frac{1}{4}} \qquad (3.14)$$

The density of the model ice was obtained by taking the ratio between the weight and the volume of the ice-sheets, Appendix 2.

3.4 Model ice properties

Representative values for the bending strength, σ_f, and the modulus of elasticity, E, were respectively taken as 20 kPa and 20 MPa. The model ice density was found to be about 530 kg/m³.

Values reported by Schwartz et al (1977), on the static modulus of elasticity, E, for saline ice range from 1.7-5.1 GPa, depending on the brine volume. With the chosen geometric scale, 1:100, our model will represent saline ice in the lower end of this range.

For correct scaling of the flexural strength the model bending strength should have been in the range of 0.3-0.7 MPa. This indicates that the bending strength in our experiments is approximately 3-7 times higher than it should have been according to the geometric scaling factor.

4. EXPERIMENTAL TECHNIQUES

The experiments were carried out in the main wave tank at Memorial University. The tank, as shown on Fig. 6, is about 58 m long, 4.5 m wide and has a maximum operating depth of 1.9 m. This tank is equipped with an MTS piston type wave generator which, for this experiment, was used to generate regular waves.

The width of the tank was divided up into three compartments over a total length of 4.9 m, Fig. 7 and 8. This was done mainly to reduce the production time and costs for an ice sheet.

The dividing walls were made up from standard sheets of plywood of size 1220x 2440x20 mm and were hung in between the tank's two catwalks. Necessary stiffness of this construction in both the longitudinal and transverse direction were obtained by running a 2"x4" beam along the whole length of the wall. Furthermore the dividing walls were braced against each other and against the wave tank's concrete walls. To overcome the buoyancy effect, lead was bolted to the bottom of each dividing wall. The final construction was then exposed to very large waves compared with the waves used in the experiments so that any vibration of the walls could be detected.

The water depth for the present study was kept constant at 0.44 m. Waves with heights up to 2 cm and periods up to 1.0 s were generated in the tank. Using the chosen scale factor, the water depth will correspond to a prototype depth of 44 m, the sheet thickness from 1.1 m to 1.8 m, the wave periods from 4.85 to 10 s and the wave heights from 1 to 2 m.

4.1 Instrumentation

Free surface waves were measured at four different locations using standard twin wire linear resistance wave probes. Two wave probes were located at the extension of the ice sheet's centre line with one probe immediately in front of the sheet and one positioned immediately behind the ice sheet. The remaining two wave probes were positioned along the centre line of either of the two side channels, Fig. 7. This made it possible to measure both the incident and transmitted waveheight. In addition to that an estimate of the natural wave decay due to viscous and frictional effects over the entire length of the ice sheet could be obtained. The measured open water wavelengths, truly represent the open water dispersion relation (Muggeridge et al., 1980).

The wave motion within the ice sheet was measured using five linear rotary potentiometers positioned as shown in Figs. 7 and 8. One end of a string (soft wire) was fixed to the ice surface by wax sealed with epoxy glue, while the other end was wrapped around a low friction pulley fixed to the rotary potentiometer's shaft and then attached to a small counterweight, 15 g, that kept the string in tension at all times, Fig. 9.

During all the tests, there was no evidence of surface drift of the continuous plate.

The time series from the four wave probes and five potentiometers were recorded on tape using two Hewlett Packard eight-track instrumentation tape recorders.

4.2 Calibration

Immediately prior to each experiment the wave probes were calibrated by taking a reading for each centimeter over a section of seven centimeters. For control a calibration test was occasionally done after an experiment. No change in calibration before and after an experiment was ever found. The sensitivity of each wave probe was assumed to be better than 0.01 V which corresponds for the least sensitive probe to about 0.025 mm. The linearity of all the probes could always be expressed by a correlation coefficient better than 0.99.

The five potentiometers were calibrated both before and after the experimental program. No change in calibration was detected, except for potentiometer #1 where a 6% change was observed. The calibration was carried out over the potentiometer's entire range with a reading for each 2.5 mm, using a micrometer with a resolution of 0.025 mm. During the calibration tests the sensitivity of the potentiometers was always better than 0.003 V, which corresponds to 0.098 mm. The linearity of the potentiometers over their entire range could always be expressed by a correlation coefficient better than 0.999.

The static calibration tests reported above were found to be sufficient, since the frequency of the input wave is much less than the frequency response of the rotary potentiometers and the associated signal processing equipment.

4.3 Data analysis

The calibrated recorded signal $X_j(t)$ at each station and the horizontal distance between the stations are sufficient to determine the wavelength inside the ice cover. Let $X_j(t)$ and $X_{j+1}(t)$ be time-series recorded at stations j and j+1, then the transfer function, $H(\omega)$, between signal j and j+1 is given as:

$$H(\omega) = \frac{X_{j+1}(\omega)}{X_j(\omega)} = A\, e^{i(\phi_2-\phi_1)} \qquad (4.1)$$

where $X(\omega)$ is the Fourier transform of $X(t)$, A is the magnitude ratio between signal j+1 and j and $(\phi_2-\phi_1)$ is the phase difference between the two signals. The wavelength, λ, inside the ice cover is then given as:

$$\lambda = \frac{2\pi}{\phi_2-\phi_1}\,\Delta x \qquad (4.2)$$

where Δx is the horizontal distance between the two stations j and j+1.

The amplitude at any station, j, inside the ice cover for regular waves was obtained from the energy, E, in the one-sided power spectrum Sp., as:

$$A_j = (4\, E_j)^{\frac{1}{2}} \qquad (4.3)$$

In eq. 4.3, E_j is the integral of the components of the single sided power spectrum. The case of a regular sinusoidal wave is handled by integrating it only over the positive domain of the signal and the result then added up for the negative portion of the signal.

5. RESULTS AND DISCUSSION

In Fig. 11 the ratio between the wavelength inside the ice sheets determined from experiments, and the open water wavelength is shown for the various wave periods used in the experiments. Theoretical curves for the flexural gravity wave, obtained from solving eq. 2.10 for the various sheet thicknesses, are also shown on the same figure using a value for the modulus of elasticity of 20 kPa and Poisson's ratio of 0.3. Good agreement exists for sheet thicknesses of 11 and 18 mm wnile for the 15 mm sheet the wavelengths inside the ice cover are consistently lower than those computed.

In using the phase shift informations to calculate the wavelength inside the ice cover as given in eq. 4.2, it was observed that the phase shift over the distance between potentiometers one and two, see Fig. 7, gave wavelengths far less than that predicted by eq. 2.10. However, the wavelength calculated using the phase shift between the potentiometer 2 and 3 or 2 and 4 or 3 and 4 or other downstream potentiometers as shown in Fig. 11 are in good agreement with that theoretically predicted by eq. 2.10. By closely watching the ice-edge during an experiment it was observed that the incident gravity wave did not become a pure sinusoidal flexural gravity wave once it entered the ice cover. Especially with the interaction of steeper waves with the thinner ice sheets it appeared as though the leading edge of the plate moved up and down as a rigid body hinged at some distance into the ice cover. This may be explained by the

existence of evanescent waves near the ice edge. In addition to the two waves local to the ice edge as given by eq. 2.12, there must, as pointed out by Wadhams (1983), be other waves present. With the solution for Φ_1 and Φ_2 as given in eq. 2.5 and 2.9 only surface fitting of the velocity potentials at the region 1/region 2 boundary plane is possible. However, no unique method to determine these additional potentials exists, which implies that the energy transmission process at the leading ice edge is not fully known.

The ratios between measured values of incident wave amplitude and that in the ice at different distances into the ice sheet for the three different sheet thicknesses used, are shown in Figs. 13, 13 and 14. The general trend is that the rate of attenuation increases with decreasing wave periods for all ice sheets, and that the rate of attenuation closely fits an exponential decay. This agrees well with the earlier laboratory studies reported by Ofuya and Reynolds (1967). They did, however, use polyethylene sheets to simulate continuous ice fields, whose elastic modulus was about 1.1 GPa which correspond to the range of values of Young's modulus, E, of sea ice. Furthermore, the attenuation rate can be seen to be a function of the sheet thickness, with increasing attenuation rate for increasing thickness. The measured wave amplitudes inside the ice cover are for continuous sheets before the initiation of visible cracks.

Due to the lack of field data no comparison of the amplitude attenuating effect of a continuous ice cover can be made with our laboratory data. However, as stated in section 2.2 it is commonly assumed that the major energy loss inside a continuous ice cover is due to creep. In an attempt to verify this an energy balance was set up as given in Appendix 3. The total energy loss is here assumed to consist of the three components E_o, E_l and E_{cr}, where E_o is the energy dissipation in waves in a viscous fluid, E_l is the energy dissipation in waves due to shear at the ice/water boundary and E_{cr} is the energy loss within the ice sheet due to creep. By applying this approach to the laboratory data, it was found as shown in Appendix 3, that the energy loss due to creep always contributed to more than 99% of the total energy loss.

A comparison of the extrapolated values of the laboratory data with field data from a pack ice field was made. The field data of Squire and Moore (1980) and Wadhams (1978) were within the extrapolated values of wave periods, but the ice thickness and water depth were very different from the values used in the present experiments. In Fig. 15 the field data of Wadhams (1975) and the extrapolated values of the laboratory data is shown. Here again it is not completely possible to make a direct comparison because Wadhams' data is obtained from a broken ice field with an ice coverage of only up to 40% for distances of 10 km from the leading ice edge. In order that his

data would simulate a 100% ice coverage he calculated an effective length, x_e, into the ice cover by decreasing the real distance according to the coverage percentage. The attenuation rate for an ice field extrapolated from the laboratory data is about one order of magnitude higher than that given by the field data of Wadhams (1975). This discrepancy can be attributed to many factors, the main one being the fact that in a continuous ice cover the main energy dissipation is due to creep while in an open pack ice field multiple scattering between the ice floes is the major energy dissipating mechanism. Furthermore, in the field there is always added energy to the ice/water system from the atmosphere, which also Wadhams' (1975) data points seem to indicate. Besides, the flow law exponent, q, which in effect described the wave amplitude decay inside the ice cover is equal to 3 for sea ice, while the results of the present model study indicate an exponential decay with q equal 1 for this model ice. Besides, as pointed out during the discussion of scaling laws, the model is properly scaled for its elastic properties while the viscous properties are not scaled exactly. Thus, the model tends to be viscoelastic rather than Glen type flow law material.

The break up process of an ice sheet as shown on Fig. 10, took place in either of two ways. For waves of large amplitude, the first wave propagating through the ice sheet would break the sheet over its entire length into strips of fairly equal length and with width equal to the width of the ice sheet. As waves continued to propagate through this broken ice field, the floes closest to the leading ice edge

would break into square floes. Then the next strip would break into smaller floes of approximately square form. This process would continue until the entire ice field consisted of floes of more or less square form and with increasing floe size with distance into the ice field. For waves with smaller amplitude only a front strip would break off, this piece would then be broken into several square floes before the next strip broke off. This process would continue until the entire ice sheet was broken up. However, as the distance into the ice sheet increased the strips would maintain their strip shape and did not easily rotate and break into square shaped floes. For waves with higher energy the former break up process took place, while the latter break up process was particularly evident for low energy waves entering the thicker ice covers. It is possible that the flexural gravity wave by itself had a sufficient amplitude to break off the first strip, but not the second one due to the high attenuation rates for short period waves in thick ice covers. An alternate hypothesis is that the flexural gravity wave in itself did not have the necessary energy to fracture the sheet, but with the added energy from the propagating wave local to the ice edge the total energy was sufficient to break off the first strip. When this first strip was broken into square floes there would be a new leading ice edge for the continuous ice cover and the same process would be repeated.

Estimates for the stress at fracture were calculated assuming elastic sinusoidal deformation of the ice sheet and using the experimentally determined wavelengths. A high estimate for the stress at fracture is 39 kPa, while 25 kPa is a low estimate. This agrees fairly well with the experimentally determined bending strength of the model ice.

The natural frequency of each ice sheet was estimated by treating the sheets as elastic plates on elastic foundation. The natural frequency of the first mode for the thinnest plate is about 6.5 Hz and 5.1 Hz for the thickest plate. These frequencies are about three times above wave frequencies used in the experiments and hence no resonant phenomena were observed.

Due partly to the tedious processes involved and the time required in casting an ice plate, the number of individual experiments carried out is not large. However, multiple experiments were carried out for that part of the experimental program dealing with the estimation of the strength properties of ice, as can be seen in Appendix 2.

6. SUMMARY AND CONCLUSIONS

A laboratory study of the interaction between a continuous ice cover and gravity waves has been carried out using recently developed artificial ice. A comparison of the measured experimental data on the wave characteristics with that of computed values indicated that this model ice can be used for simulation of wave propagation in ice covered seas. The wave attenuation of flexural-gravity waves propagating through a continuous ice cover has also been measured and compared with field data. Qualitative agreement between field and experimental data exists.

The energy loss due to creep in a continuous ice cover is shown to contribute to more than 99% of the total energy loss inside the ice cover.

Furthermore it can be concluded that the break up process of a continuous ice cover can be studied in the laboratory using this model ice.

REFERENCES

Arunachalam, V.M., Grande, O. and Muggeridge, D.B., 1983, "Padé Coefficients for the Solution of the Wave Dispersion Equation Under Ice". Communicated to Ocean Engineering Journal.

Bates, H.F. and Shapiro, L.H., 1980a, "Breaking Ice with Gravity Waves", Journal of Energy Resources Technology, Transactions of American Society of Mechanical Engineers, Vol. 102, No. 3, pp. 148-153.

Bates, H.F. and Shapiro, L.H., 1980b, "Long-Period Gravity Waves in Ice-Covered Sea", Journal of Geophysical Research, Vol. 85, No. C2, pp. 1095-1100.

Bates, H.F. and Shapiro, L.H., 1981, "Plane Waves in Visco-elastic Floating Ice Sheet", Journal of Geophysical Research, Vol. 86, No. C5, pp. 4269-4273.

Carter, D., 1978, "Wave Propagation in Ice-Covered Waters", Report No. TP 1522 to Transport Canada, Research and Development Centre, Technology Applications Division, 33 pp.

Grande, O., Arunachalam, V.M. and Muggeridge, D.B., 1983, "Model Tests of Wave Attenuation in Ice", Proceedings of the Seventh International Conference on Port and Ocean Engineering under Arctic Conditions, Helsinki, Finland, Vol. 3.

Hetényi, M., 1946, "Beams on Elastic Foundation", Ann Arbor, The University of Michigan Press, pp. 1-26.

Keliher, T.E., 1976, "An Investigation of the Effect of Large-Amplitude Ocean-Waves on Antarctic Pack Ice", Arctic Ice Dynamics Joint Experiment Bulletin, No. 34, pp. 114-135.

Michel, B., 1978, "Ice Mechanics", Quebec, Les Presses de l'Universite Laval, pp. 438-478.

Muggeridge, D.B., Chen, C.M. and Murray, J.J., 1980, "Calibration of a 58 m Wave Flume and an Initial Study of a Circular Cylinder to Sinusoidal Waves". Internal report, Faculty of Engineering, Memorial University of Newfoundland, St. John's, 32 pages.

Ofuya, A.O. and Reynolds, A.J., 1967, "Laboratory Simulation of Waves in an Ice Floe", Journal of Geophysical Research, Vol. 72, No. 14, pp. 3567-3583.

Schwartz, J. and Weeks, W.F., 1977, "Engineering Properties of Sea Ice", Journal of Glaciology, Vol. 19, No. 81, pp. 499-531.

Schwartz, J. Frederking, R., Gavrillo, V., Petrov, 1.6, Hirayama, K.I., Mellor, M., Tryde, P., and Vaudrey, K.D., 1981, "Standardized Testing Methods for Measuring Mechanical Properties of Ice", Cold Region Science and Technology, Vol. 4, No. 3, pp. 245-253.

Squire, V.A. and Allan, A.J., 1980, "Propagation of Flexural Gravity Waves in Sea Ice, Sea Ice Processes and Models", University of Washington Press, pp. 327-337.

Squire, V.A. and Moore, S.C., 1980, "Direct Measurement of the Attenuation of Ocean Waves by Pack Ice", Nature, Vol. 283, No. 5745, pp. 365-368.

Timco, G.W., 1981, "On the Test Methods for Model Ice", Cold Region Science and Technology, Vol. 4, No. 3, pp. 269-274.

Wadhams, P., 1973, "Attenuation of Swell by Sea Ice", Journal of Geophysical Research, Vol. 78, No. 18, pp. 3552-3561.

Wadhams, P., 1975, "Airborne Laser Profiling of Swells in an Open Ice Field", Journal Geophysical Research, Vol. 80, No. 33, pp. 4520-4528.

Wadhams, P., 1978, "Wave Decay in the Marginal Ice Zone Measured from a Submarine", Deep Sea Research, Vol. 25, No. 1, pp. 23-40.

Wadhams, P., 1983, "The Seasonal Ice Zone", from The Geophysics of Sea Ice, (N. Untersteiner, ed.), Plenum Press, in press.

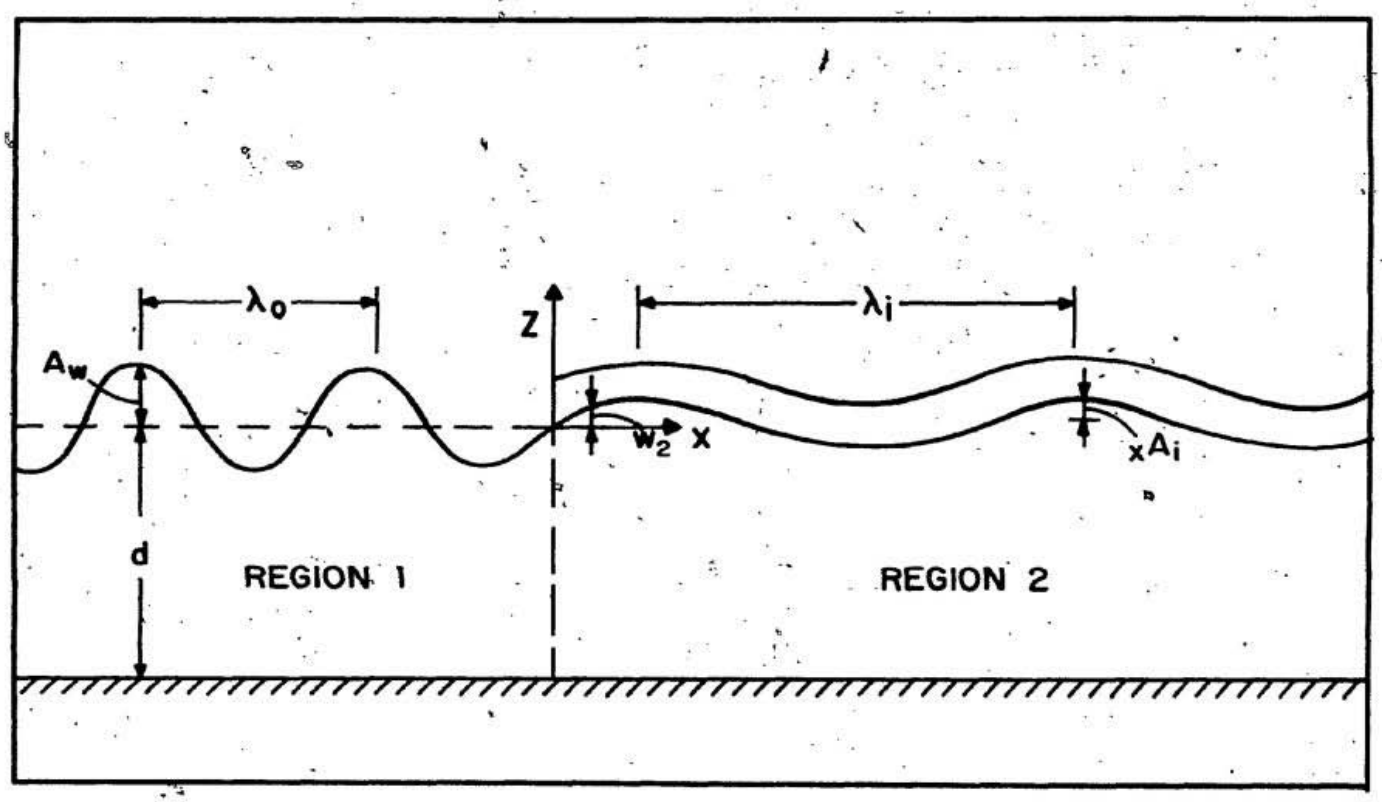

Fig. 1. Schematic representation of wave entering an ice cover.

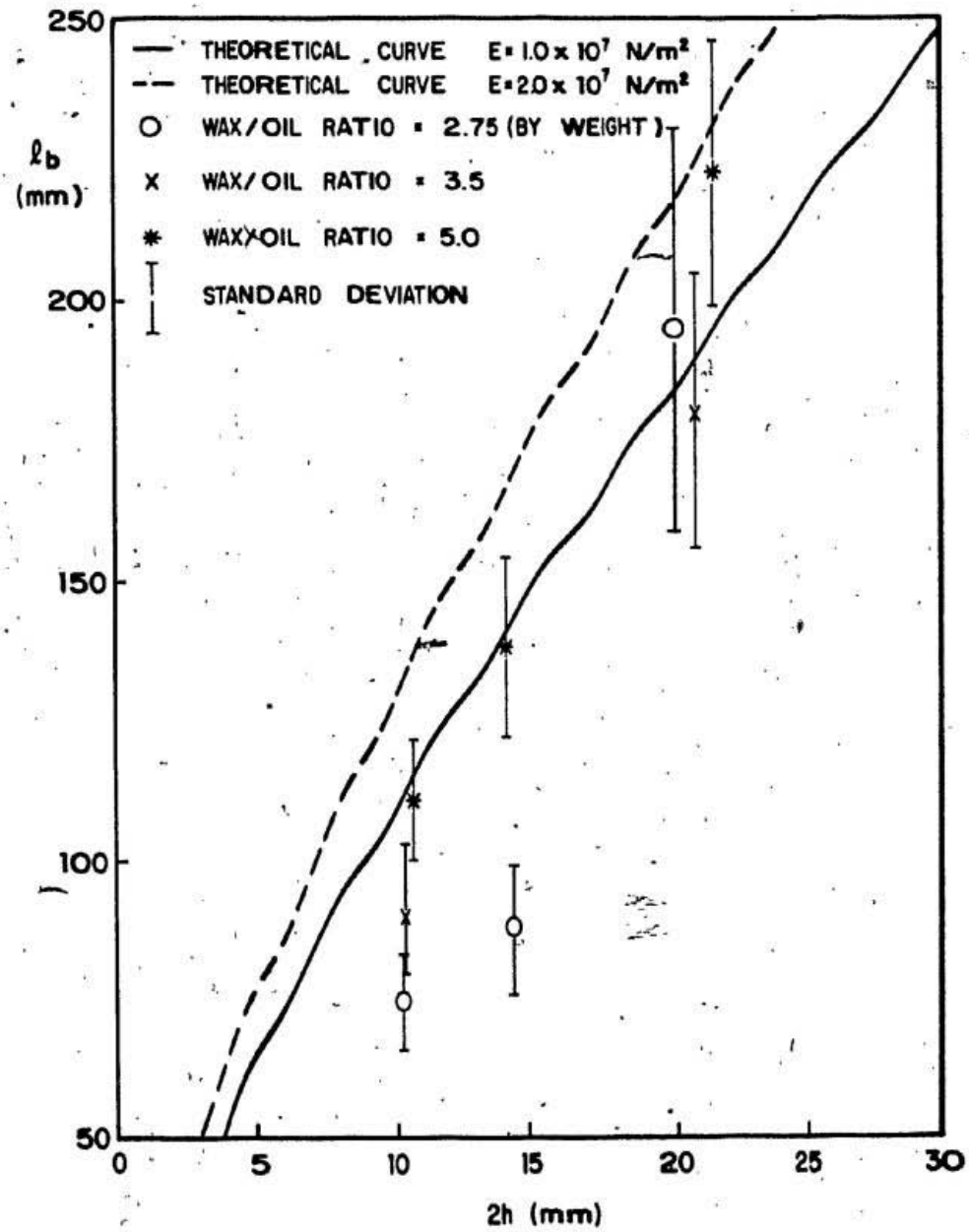

Fig. 2. Breaking length versus model ice thickness for different wax/oil ratios.

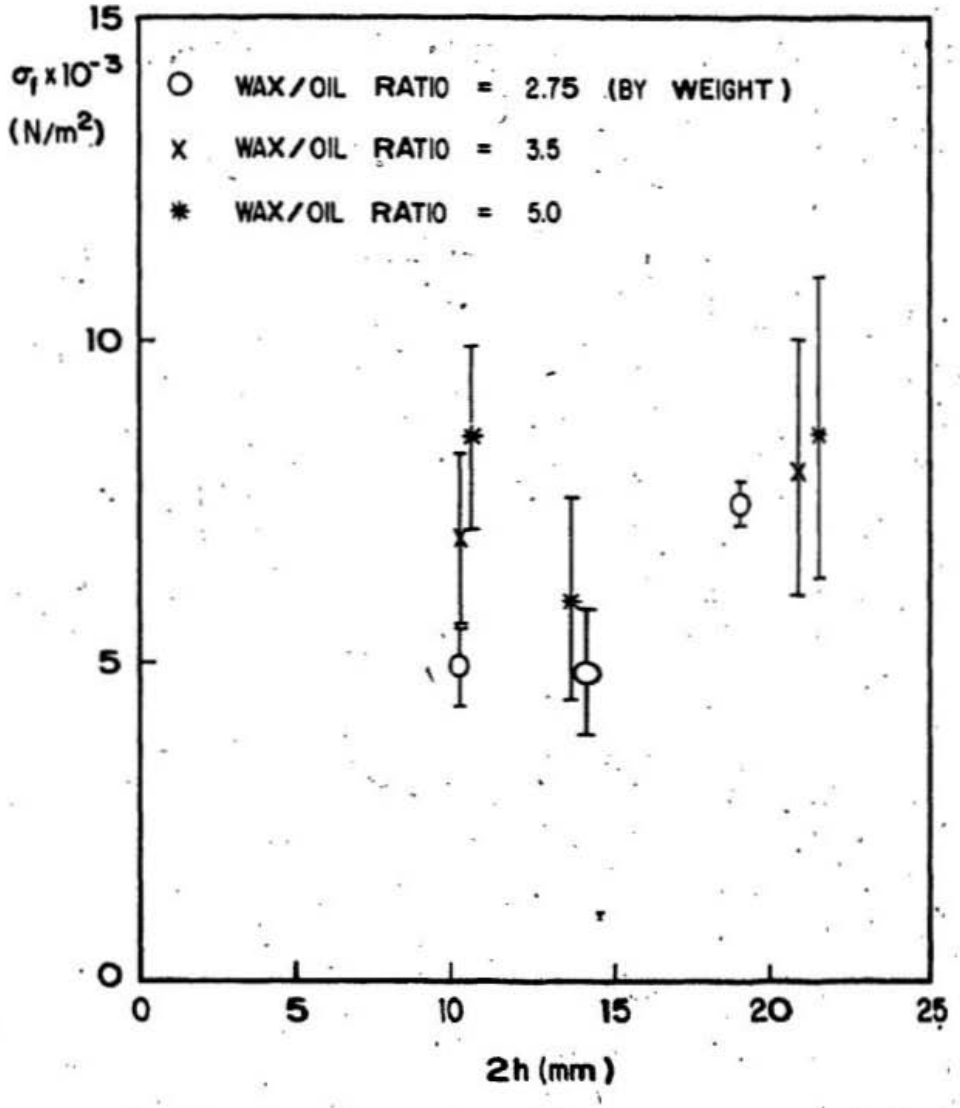

Fig. 3. Bending strength versus model ice thickness for different wax/oil ratios.

Fig. 4. Cantilever beam test.

Fig. 5. Load-deflection test of model ice sheet.

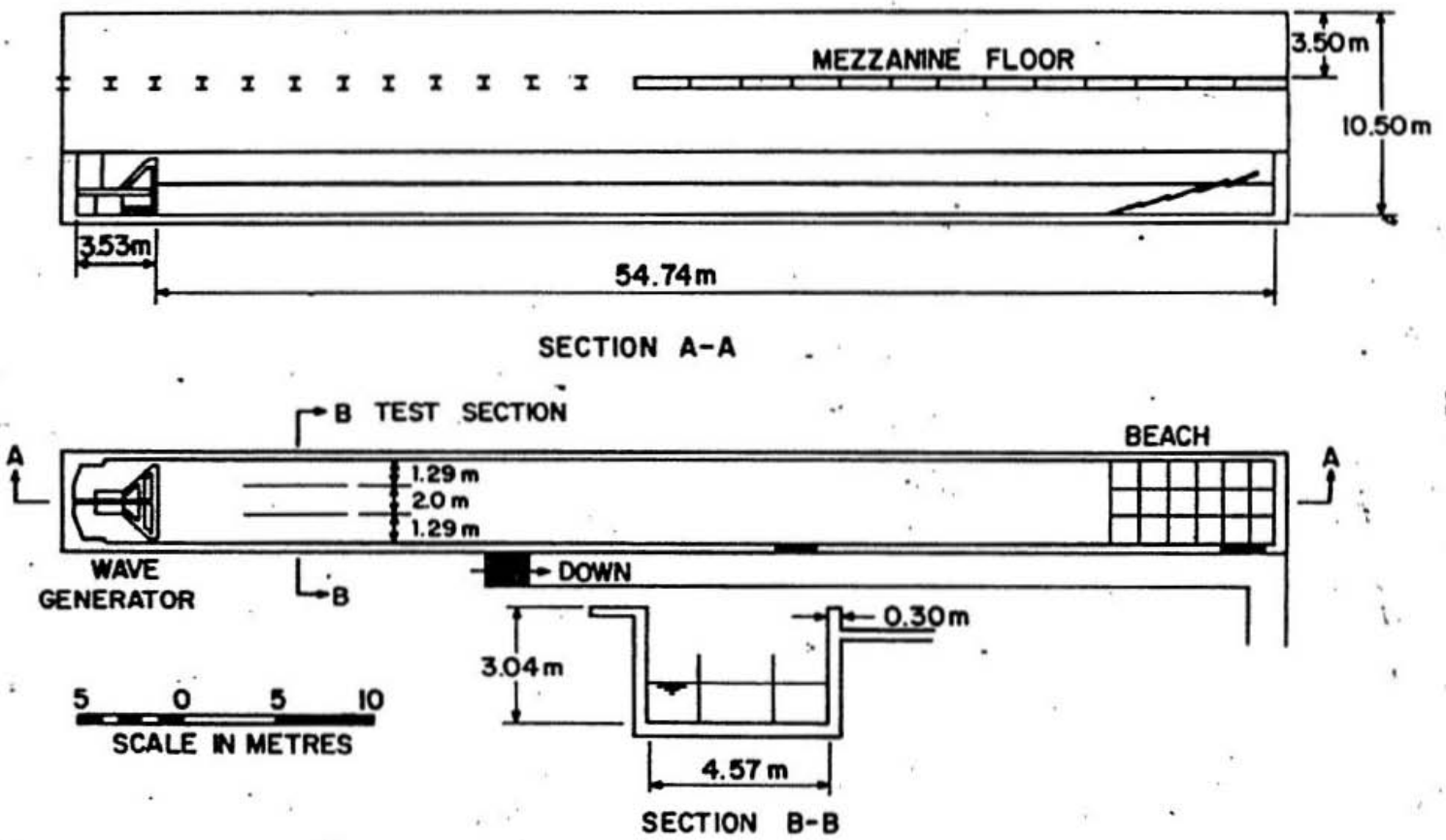

Fig. 6. Elevation and plan views of wave tank.

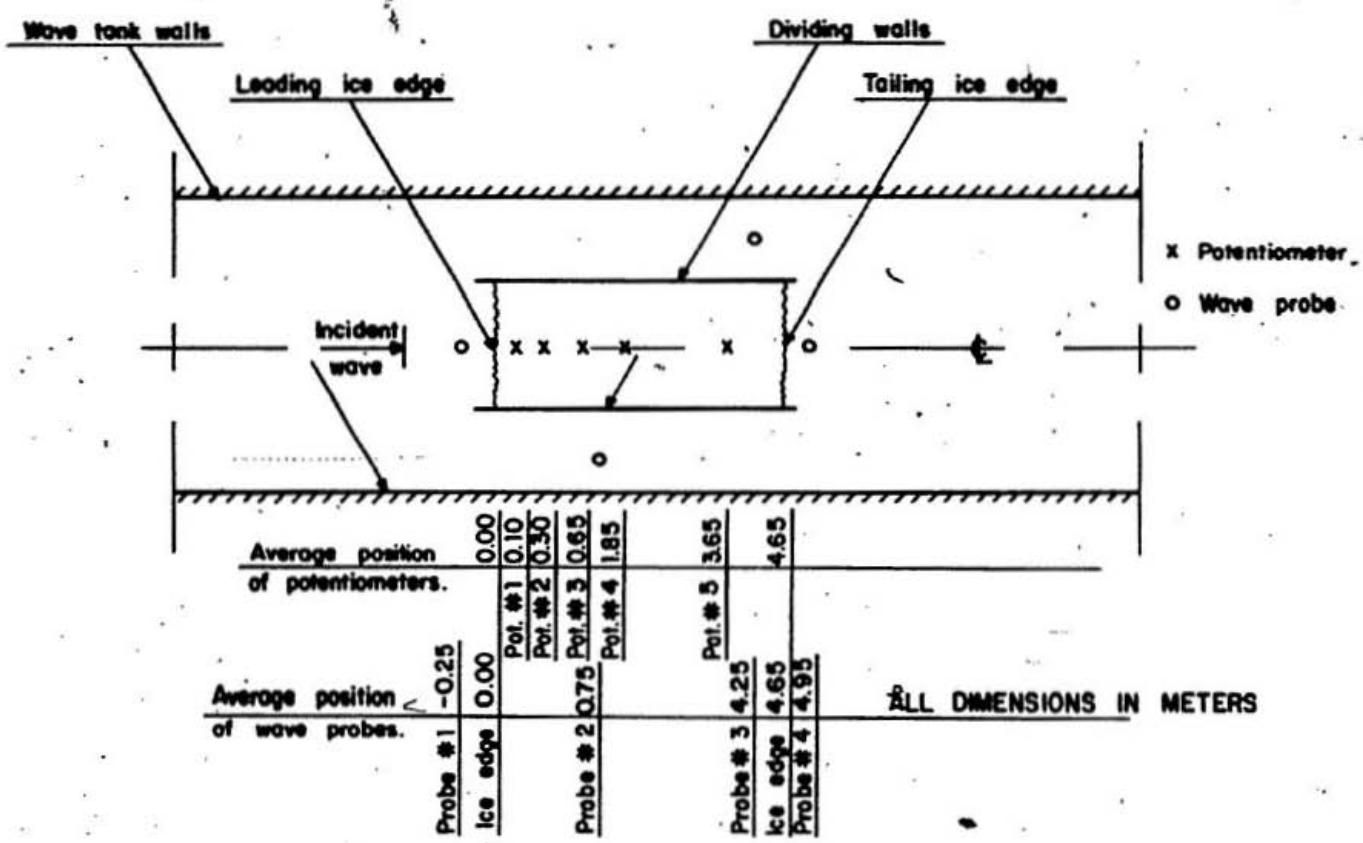

Fig. 7 Experimental configuration and instrumentation.

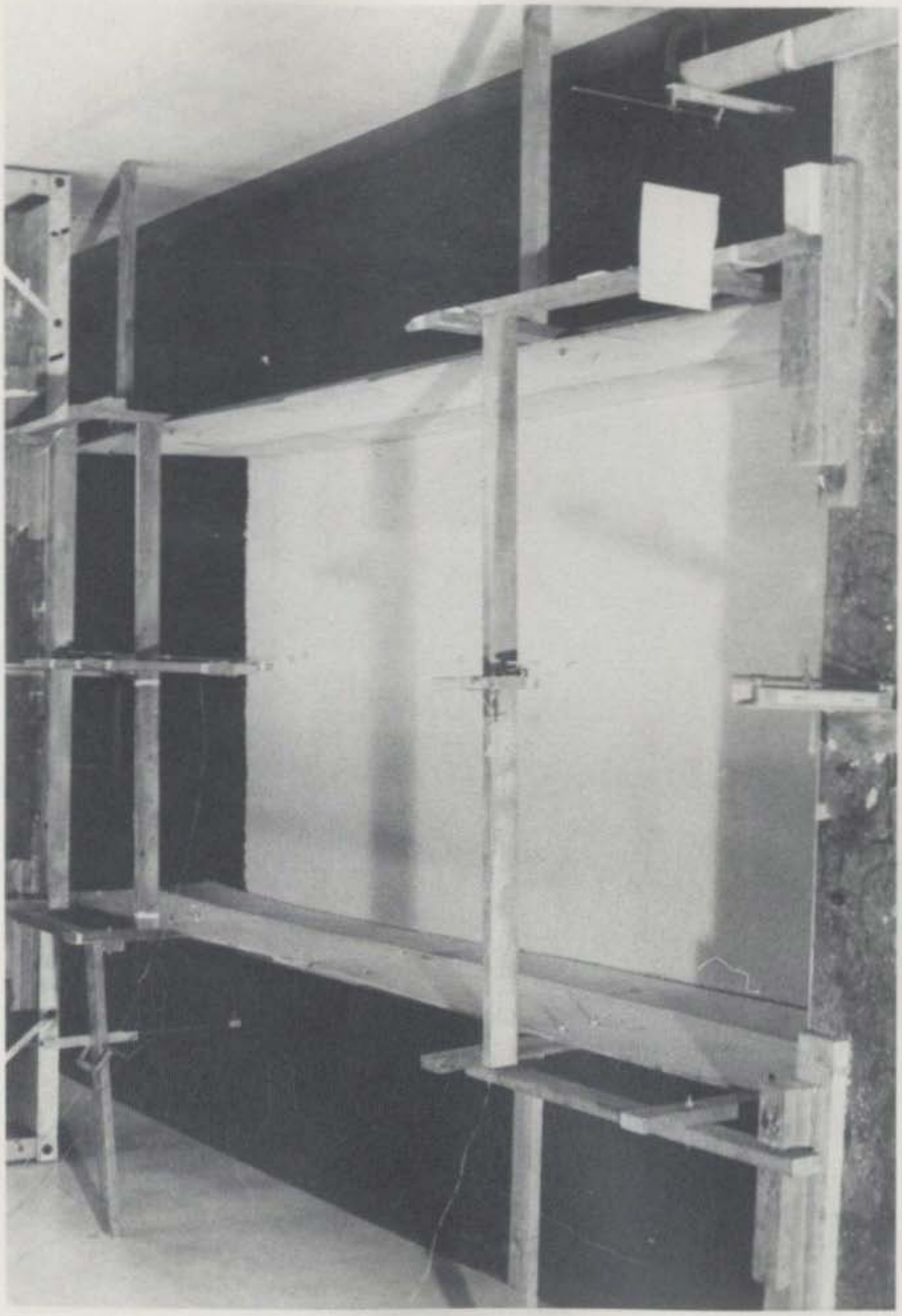

Fig. 8. Model ice sheet.

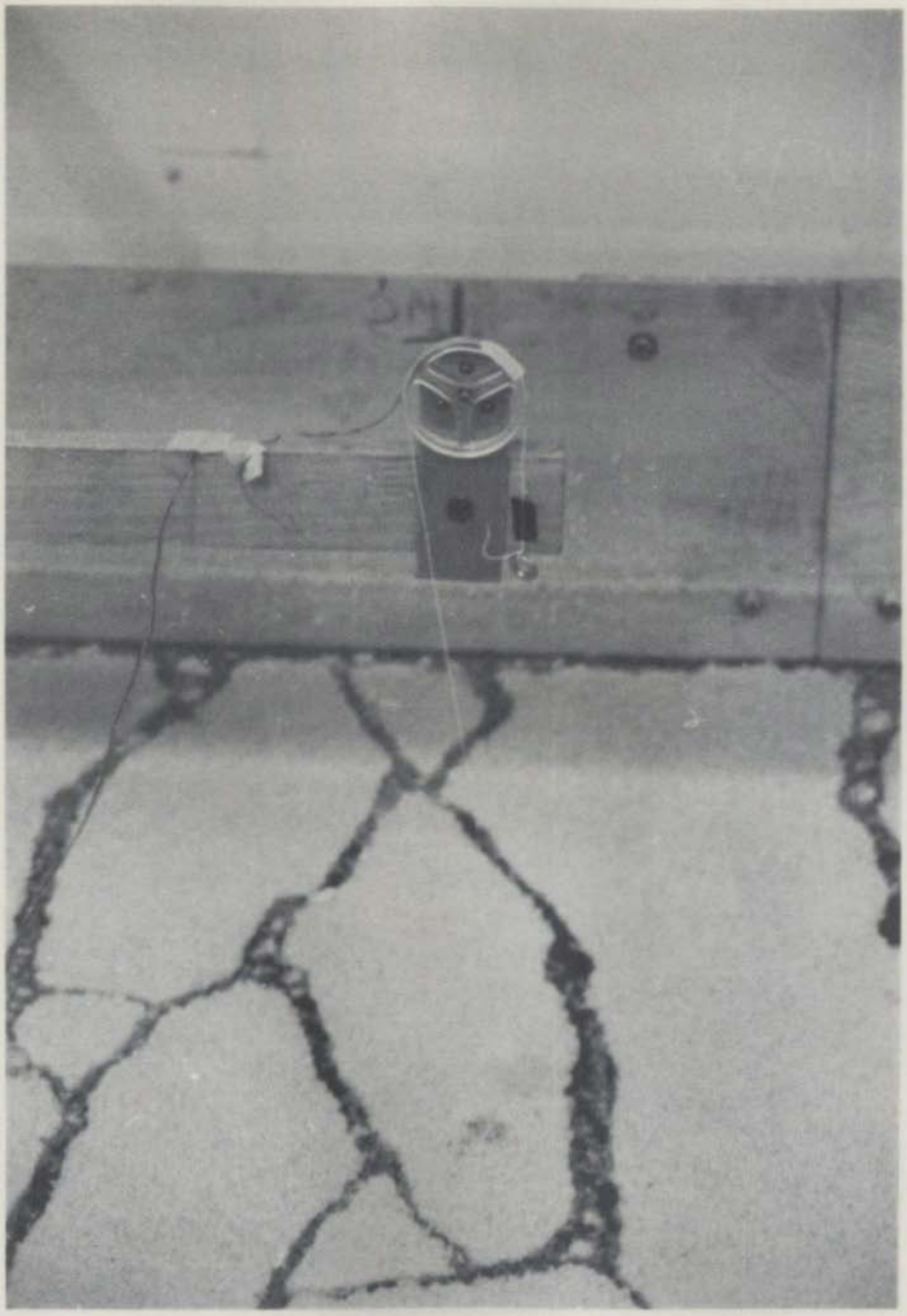

Fig. 9. Vertical displacement transducer.

Fig. 10. Break up process of ice sheet

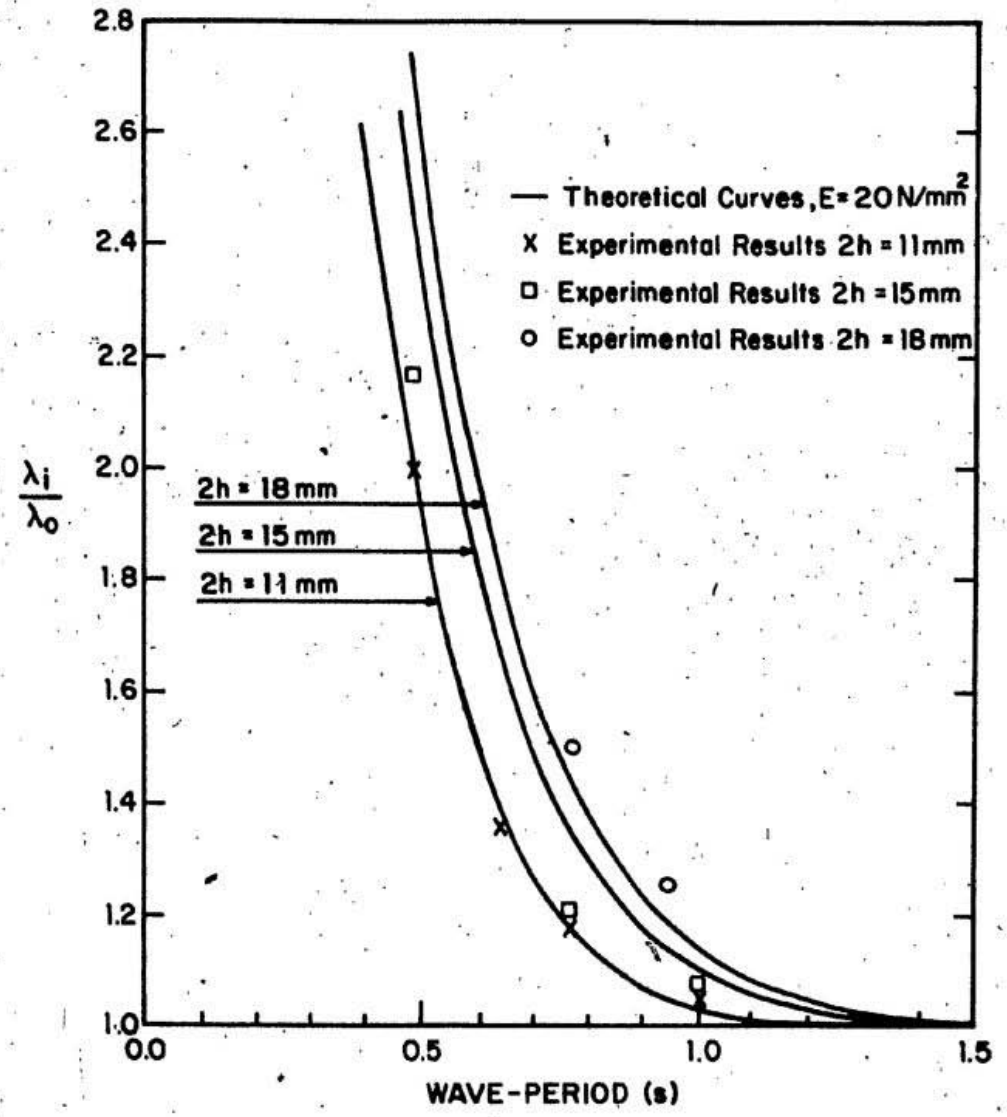

Fig. 11 Ratio between wave-length in a continuous ice sheet and in open water as a function of wave-period and sheet thickness.

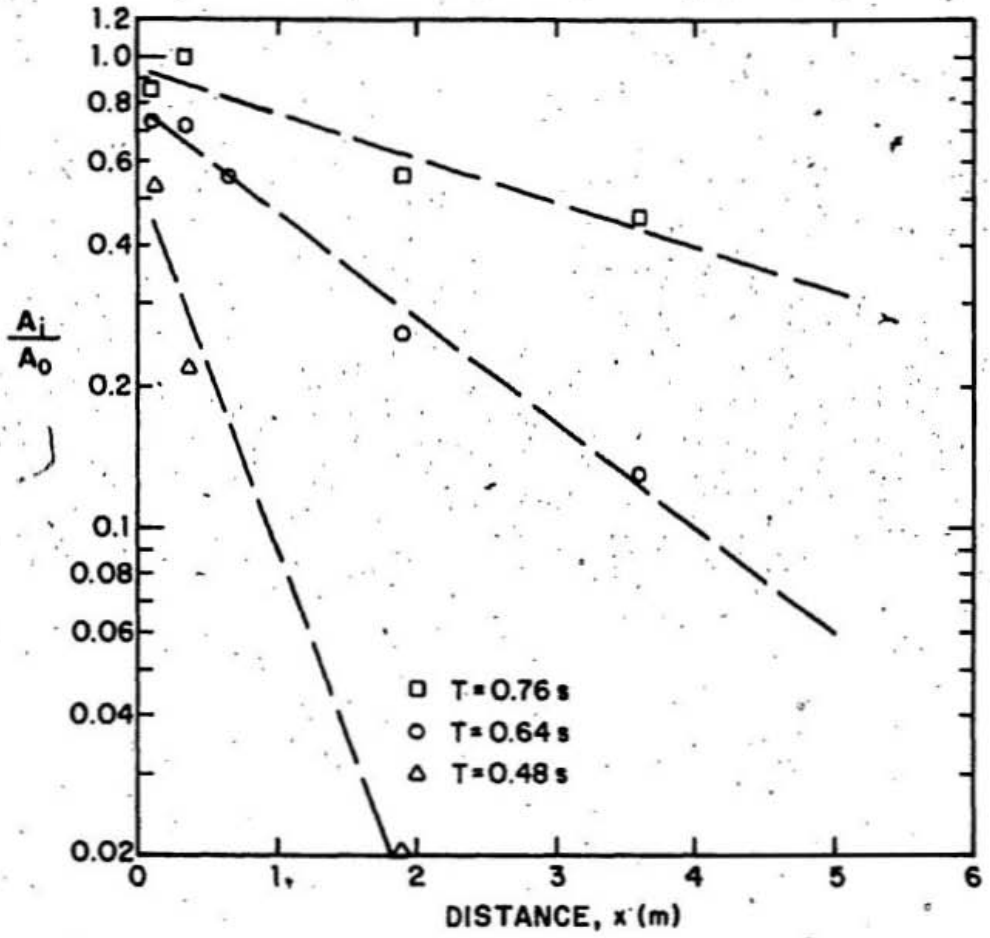

Fig. 12 Wave attenuation, continous ice cover, 2h = 11 mm.

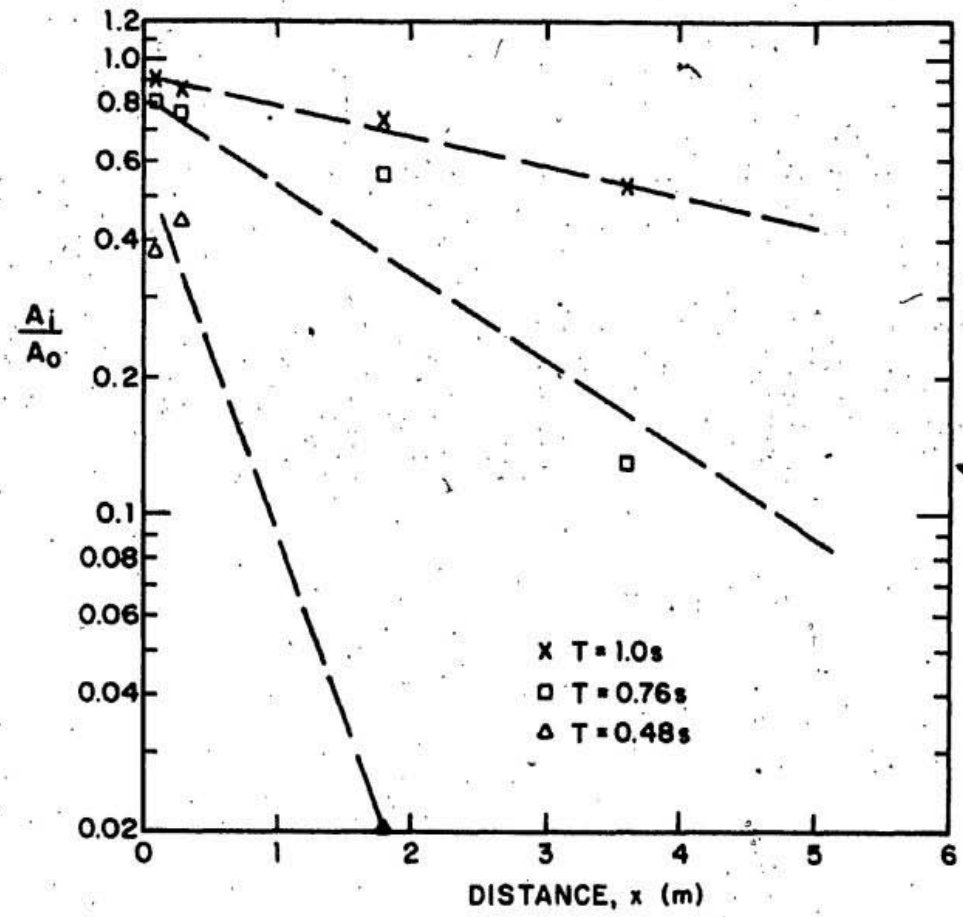

Fig. 13 Wave attenuation, continous ice cover, 2h = 15mm.

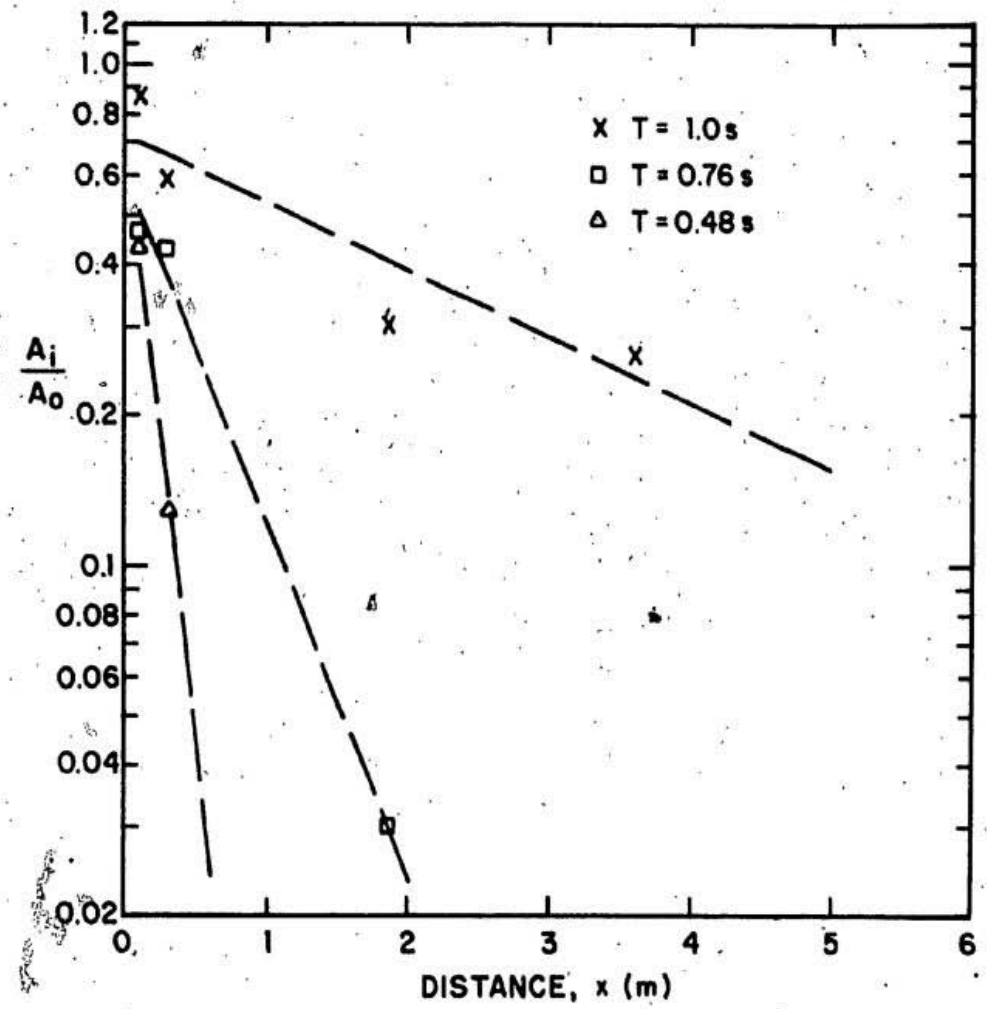

Fig. 14 Wave attenuation, continous ice cover, 2h = 18 mm.

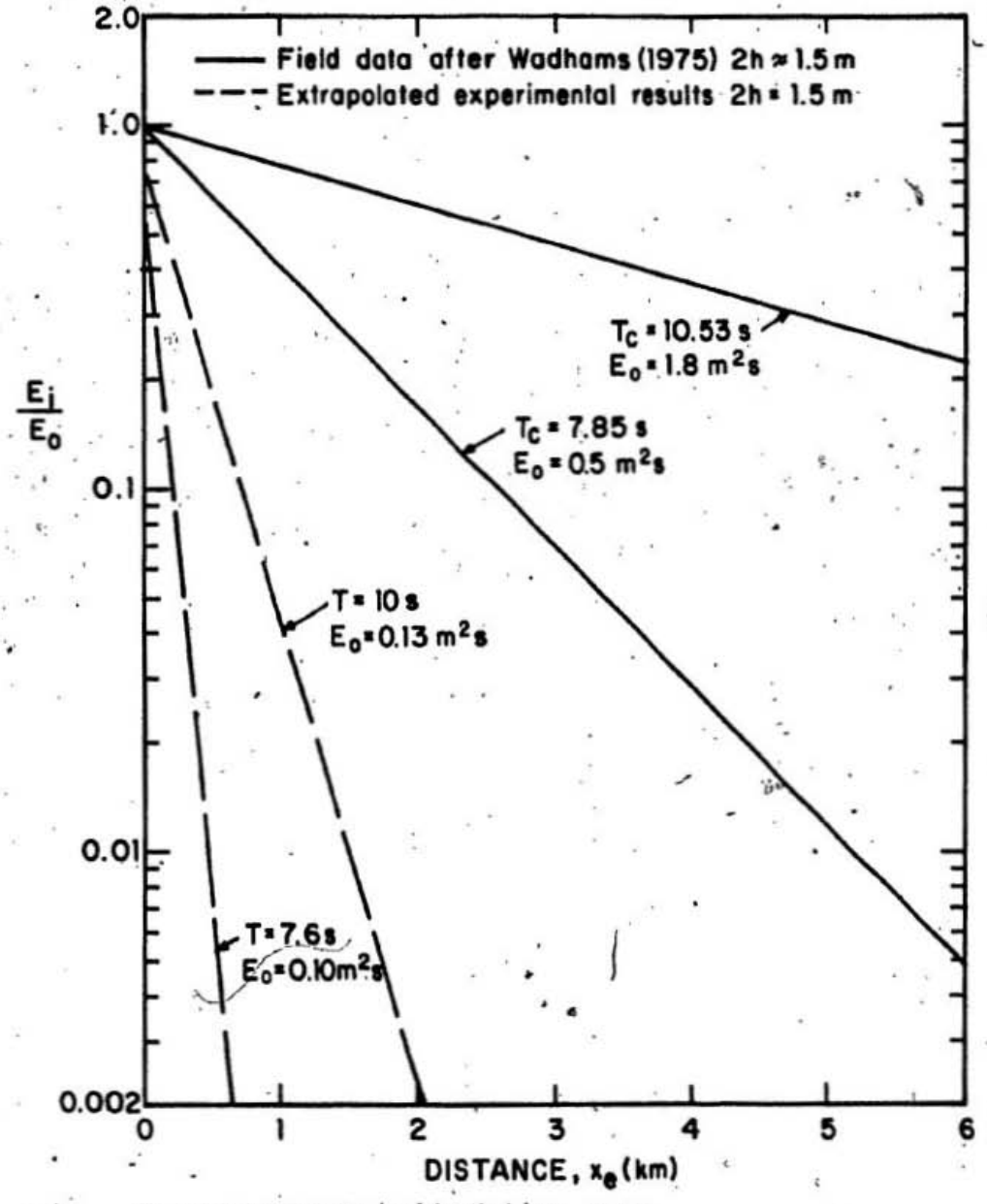

E_i = Wave energy inside the ice-cover
E_0 = Open water wave energy

Fig.15 Wave energy decay as a function of distance

APPENDIX 1

EVANESCENT WAVES NEAR THE LEADING ICE EDGE

To obtain eq. 2.12, we proceed from eq. 2.9 which is rewritten as

$$\phi_2 = \sum_{j=1}^{5} [A_j e^{ik_j x} + B_j e^{-ik_j x}] \frac{\cosh k_j(z+d)}{\cosh k_j d} e^{-i\omega t} \quad (A1)$$

Neglecting the terms corresponding to the flexural-gravity wave, and the terms arising from the two complex wave numbers which have positive real part (since they lead to potentials that are increasing indefinitely with depth) and expanding of eq. A1 in terms of a's and b's yields then:

$$\phi_2' = [[A_1 e^{-(b+ia)x} + B_1 e^{(b+ia)x}] \frac{\cosh(-a+ib)(z+d)}{\cosh(-a+ib)d} + [A_2 e^{(b+ia)x} + B_2 e^{-(b-ia)x}] \frac{\cosh(-a-ib)(z+d)}{\cosh(-a-ib)d}] \cdot e^{-i\omega t} \quad (A2)$$

The two terms B_1 and A_2 are physically undefined since they are exponentially unbounded at $x = \infty$. Eq. A2 can then be reduced to:

$$\phi_2' = [A_1 e^{-(b+ia)x}[\cosh(-az-2ad+ibz)+\cosh(-az+2ibd+ibz)] + B_2 e^{-(b-ia)x}[\cosh(-az-2ad-ibz)+\cosh(-az-2ibd-ibz)]] \cdot \frac{e^{-i\omega t}}{2|\cosh(-a+ib)d|^2} \quad (A3)$$

Separation of real and imaginary parts yields:

$$\Phi_2' = [(A_1+B_2)[e^{-az-2ad}\cos(bz-ax)+e^{az+2ad}\cos(-bz-ax)$$
$$+ e^{-az}\cos(bz+2bd-ax) + e^{az}\cos(-bz-2bd-ax)]$$
$$+ (A_1-B_2)[(e^{-az-2ad}i\sin(bz-ax)+e^{az+2ad}i\sin(-bx-az)$$
$$+ e^{-az}i\sin(bz+2bd-ax) + e^{az}i\sin(-bz-2bd-ax)]]$$
$$\cdot \frac{e^{-i\omega t}}{4|\cosh(-a+ib)d|^2} \qquad (A4)$$

Eq. A4 can now be written in terms of a standing and a propagating wave as:

$$\Phi_2' = [2B_2[e^{-az-2ad}\,\mathrm{coshi}(bz-ax) + e^{az+2ad}\mathrm{coshi}(-bz-ax)$$
$$+ e^{-az}\mathrm{coshi}(bz+2bd+ax) + e^{az}\mathrm{coshi}(-bz-2bd-ax)]$$
$$+ (A_1-B_2)[e^{-az-2ad}e^{i(bz-ax)}+e^{az+2ad}e^{i(-bx-ax)}$$
$$+ e^{-az}e^{i(bz+2bd-ax)} + e^{az}e^{i(-bz-2bd-ax)}]]$$
$$\cdot \frac{e^{-i\omega t}e^{-bx}}{4|\cosh(-a+ib)d|^2} \qquad (A5)$$

or

$$\Phi_2' = [B_2[e^{-iax}(e^{-az-2ad+ibz}+e^{az+2ad-ibz})$$
$$+ e^{-iax}(e^{-az+i(bz+2bd)}+e^{az-i(bz+2bd)}) + e^{iax}(e^{-az-2ad-ibz}$$
$$+ e^{az+2ad+ibz}) + e^{iax}(e^{-az-i(bz+2bd)}+e^{az+i(bz+2db)})]$$
$$+ (A_1-B_2)[e^{-iax}(e^{az+2ad-ibz}+e^{az-2ad+ibz})$$
$$+ e^{-iax}(e^{az-i(bz+2bd)} + e^{-az+i(bz+2bd)})]] \frac{e^{-i\omega t}\,e^{-bx}}{4|\cosh(-a+ib)d|^2}$$
$$(A6)$$

This can now be written as:

$$\Phi_2' = [4B_2(e^{-iax}\cosh(az+ad-i(bz+bd))\cosh(ad+ibd)+e^{iax}\cosh(az+ad+i(bz+bd))\cosh(ad-ibd)] + 4(A_1-B_2)\, e^{-ax}\cosh(az+ad-i(bd+bz))\cosh(ad+ibd)]\, \frac{e^{-i\omega t}e^{-bx}}{4|\cosh(-a+ib)d|^2} \quad (A7)$$

Which yields the result:

$$\Phi_2' = [B_2[(\frac{\cosh(az+ad-i(bz+bd)}{\cosh(ad-ibd)} + \frac{\cosh(az+ad+i(bz+bd)}{\cosh(ad+ibd)})\cos ax + i(\frac{\cosh(az+ad+i(bz+bd)}{\cosh(ad+ibd)} - \frac{\cosh(az+ad-i(bz+bd)}{\cosh(ad-ibd)})\sin ax] + e^{-ax}\,(A_1-B_2)\,\frac{\cosh(az+ad-i(bz+bd))}{\cosh(ad-ibd)}]\, e^{-i\omega t}e^{-bx} \quad (A8)$$

Define:

$$\Omega = \frac{\cosh(az+ad-i(bz+bd))}{\cosh(ad-ibd)} \quad (A9)$$

and

$$H = \frac{\cosh(az+ad+i(bz+bd))}{\cosh(ad+ibd)} \quad (A10)$$

The final expression for Φ_2' can then be written as:

$$\Phi_2' = [2B_2(H\Omega)^{1/2}\cos(ax-\theta)\, e^{-bx} + (A_1-B_2)\,\Omega e^{-(bx+iax)}]e^{-i\omega t} \quad (A11)$$

where $\theta = \arctan\left[\frac{i(H-\Omega)}{H+\Omega}\right]$ (A12)

For deep water, $d \to \infty$, H and Ω reduce to:

$$H_\infty = e^{(a+ib)z} \tag{A13}$$

$$\Omega_\infty = e^{(a-ib)z}$$

And eq. (A11) simplifies to the deep water velocity potential given by Wadhams (1983).

$$\phi_2' = [2B_2 \cos(ax+bz)+(A_1-B_2)\ e^{-i(ax+bz)}]e^{-(bx-az)}$$

$$e^{-i\omega t} \tag{A14}$$

APPENDIX 2

PROPERTIES OF MODEL ICE SHEET

SHEET #	SIZE		THICKNESS		BENDING STRENGTH		ELASTIC MODULUS		DENSITY	LAYERS OF PELLETS
	WIDTH (m)	LENGTH (m)	2h (mm)	s (mm)	σ_f (kPa)	s (kPa)	E (MPa)	s (MPa)	ρ_i (kg/m³)	
2	2.03	4.87	14.6	0.46	23	15	32	10	527	4
3	2.03	4.87	11.4	0.50	17	8.6	-	-	508	3
4	2.03	4.87	17.6	1.16	23	5.2	39	12	547	5
5	2.00	4.87	10.8	0.69	20	7.7	28	20	543	3
6	2.00	4.87	15.2	0.82	21	8.7	31	22	514	4
7	2.00	4.87	18.2	1.35	26	14	-	-	539	5

* s = standard deviation

APPENDIX 3

ENERGY LOSSES IN A CONTINUOUS ICE SHEET DUE TO WAVE MOTION

To model the propagation of flexural gravity waves in a continuous ice sheet three scaling laws have to be satisfied simultaneously, and they are:

1. Froude number scaling to simulate body effects
2. Cauchy number scaling to simulate flexural effects
3. Reynolds number scaling to simulate viscous effects

Unfortunately, it is almost impossible to satisfy all three scaling requirements simultaneously. However, for large Reynolds numbers the viscous effects are small compared with the gravitational effect in free surface flow problems. In this experiment the fluid Reynolds number based on the average orbital particle velocity at the plate-fluid interface was $10^5 > Re > 10^4$. In this range of Reynolds numbers, the viscous effects are most likely to be of secondary importance, and therefore a scaling satisfying the first two criteria, as stated in chapter 3, is valid.

To obtain a quantitative description of the energy loss in a continuous ice sheet the energy loss balance equation B1 was assumed to be applicable.

$$E_{cr} = E_t - E_o - E_1 \qquad (B1)$$

where E_o is the energy dissipated in waves in a viscous fluid, E_1 is the energy dissipated in waves due to shear at the ice/water boundary, E_{cr} is the energy loss due to creep and E_t is the total energy loss. All the energy losses are per unit surface area and time. Expressions for E_o and E_1 for a slightly viscous fluid are given by Ofuya and Reynolds (1967) as:

$$E_o = 2\mu A^2 k^3 c^2 \qquad (B2)$$

$$E_1 = \frac{E_o}{4}\left(\frac{Re}{2}\right)^{\frac{1}{2}} \qquad (B3)$$

where μ is the dynamic viscosity, A is the wave amplitude, k is the wave number, c is the wave celerity and Re is a Reynolds number, here defined as:

$$Re = \frac{c}{\nu k} \qquad (B4)$$

where ν is the kinematic viscosity.

The total energy loss, E_t, is estimated from the measured wave amplitudes, A_i, at stations i=1 to 5

$$E_t = \frac{c_g \rho_w g Q}{2\ \Delta x}\left(A_i^2 - A^2_{i+1}\right) \qquad (B5)$$

where Δx is the distance between station i and i+1 and Q is a function as defined in the nomenclature.

The calculated ratio between the estimated energy loss due to creep and the measured total energy loss is shown in table T1.

Wave period (s)	Sheet thickness (mm)	E_t/E_{cr}	
		Between stations 1 and 2	Between stations 2 and 4
0.64	11	0.998	0.999
0.48	11	0.9999	0.9996
1.00	15	0.9994	0.9982
0.76	15	0.9992	-
1.00	18	0.9999	0.9996
0.48	18	0.9999	0.9997

END

2106H85

FIN